***Original Research Article***

# Strength and Deformation: Structural Characteristics of Concrete Beams Reinforced with GFRP Bars


## ABSTRACT

This research presents findings from experiments conducted on the structural behavior of concrete beams reinforced with Glass Fiber Reinforced Polymer (GFRP) bars and conventional steel bars as control. The mechanical properties of the GFRP bars and steel bars (10mm and 12mm nominal ~~sizes~~ diameter) used were ascertained. A total of seven (7) reinforced concrete (RC) beams measuring 120mm x 200mm x 2000mm mm were cast, six (6) of which were GFRP reinforced and one (1) was steel reinforced, and were loaded until failure. Test variables considered were the concrete compressive strength, tensile reinforcement ratios and loading conditions. The data gathered were analyzed using theoretical and experimental approach to provide an insight to structural characteristics of the RC beams cast. An estimation for the theoretical failure load from fracture of tension bars were based on a partial factor of safety ($\gamma_m$) of 1.52 for the tensile strength of GFRP. The study examined the deformational behavior including load-deflection response, crack propagation, flexural capacity and failure modes under a four-point monotonic loading test. The experimental results revealed that the GFRP RC beams exhibited typical bilinear elastic behavior under static loading with a reduction in stiffness after cracking. The GFRP RC beams failed by sudden concrete crushing due to shear-bond failure, diagonal tension failure in the concrete, and flexural failure in contrast to the steel-RC beam which failed due to yielding of the steel tension bars. The investigation further highlighted that increasing the concrete compressive strength and the longitudinal tensile reinforcement ratio of GFRP-RC beams significantly improved their structural performance, reducing crack widths and increasing failure loads. GFRP reinforced concrete beams demonstrated higher ultimate load capacities and deformations compared to steel-reinforced beams, despite their brittle failure modes. Further aligning with previous research, findings revealed that higher concrete strength leads to a greater number of cracks, but with reduced spacing and narrower widths.



**Keywords:**

GFRP bar, Reinforced Concrete Beams, Flexural Strength, Deformation Characteristics, Monotonic Loading

## 1. INTRODUCTION

The construction industry has historically been motivated by the necessity for materials that can improve structural performance while also addressing concerns related to sustainability and durability. Despite its widespread usage, traditional steel reinforcement poses various challenges, such as susceptibility to corrosion, and a substantial carbon footprint linked to its manufacturing process [1]. Glass Fiber Reinforced Polymer (GFRP) bars have emerged as a promising substitute in response to these challenges, offering superior properties like a high strength-to-weight ratio, exceptional corrosion resistance, appreciable performance against fatigue, non-conductivity, electromagnetic resistivity and durability [2 - 4].

GFRP bars consist of continuous glass fibers incorporated in a polymer matrix, typically epoxy or vinyl ester resin [5]. This composition provides several benefits, including non-corrosive characteristics, which are especially advantageous in settings prone to chemical exposure or moisture, like marine structures, bridges, and wastewater treatment facilities [6]. Moreover, the remarkable tensile strength of GFRP bars renders them an appealing choice for tasks necessitating lightweight yet ~~sturdy~~ (study) reinforcement [4].

Despite the advantages mentioned, the integration of GFRP bars into construction practices has been gradual, mainly due to the limited comprehension of their long-term performance and response under diverse loading conditions. Recent research efforts have concentrated on clarifying the mechanical features of GFRP-reinforced concrete structures, leading to notable progress in understanding their tensile strength, bonding behavior, and flexural capacity [7, 8]. According to Boateng et al. [7] and Issa et al. [9], the GFRP reinforcing bars show a relatively lower modulus of elasticity, reduced ductility, and decreased stiffness when compared to traditional steel. This reduced stiffness, in conjunction with various factors such as altered bond characteristics and decreased tension stiffening, leads to deformations that exceed those of steel-reinforced elements at all loading stages. As a result of these significant deformations, the design of structures might be influenced by constraints related to deflection [10]. Nonetheless, extensive investigations on the strength and deformation properties of GFRP-reinforced beams remain relatively scarce.

The strength of a reinforced concrete beam is a crucial parameter that determines its capacity to sustain loads without any structural failure [11]. In the instance of GFRP-reinforced beams, this covers not just the ultimate load-carrying capability but also the beam's response under various load forms. On the contrary, deformation characteristics offer valuable insights into

how a beam reacts to applied loads concerning deflections and crack development [12, 13]. The comprehension of these characteristics is essential in evaluating the serviceability and durability of GFRP-reinforced beams. Unlike steel, GFRP bars display a linear elastic response until failure without yielding, influencing the ductility and energy absorption potential of the reinforced concrete structures [7, 14, 15].

Experimental and numerical investigations have revealed that the incorporation of GFRP bars led to improvements in the flexural strength of concrete beams, where different reinforcement ratios had varying impacts on load-bearing capacity and deflection [16]. Results from the studies showcased promising outcomes for the use of GFRP bars in concrete structures, demonstrating higher failure loads and deflections compared to traditional steel reinforcement, particularly in cases involving lower strength concrete beams [17]. The findings also highlighted the variation in behavior of GFRP-reinforced concrete beams based on longitudinal reinforcement ratios, indicating that the role of GFRP bars in the compression zone was negligible in design considerations. Adam et al. [18] concluded that increasing the concrete strength and the reinforcement ratio of GFRP-RC beams can lead to a substantial improvement in their flexural performances as they can reduce the crack widths. Zhang et al. [19] researched on the bonding performance between GFRP bars and reported that concrete is significantly affected by the deformation characteristics of the bars, where higher deformation coefficients can enhance bond strength but may result in a transition of failure modes from ductile to brittle. Xie et al. [20] also had similar findings.

Muhamad [21] made an experimental inquiry involving full-scale assessments of GFRP-reinforced beams under controlled settings and furnished significant insights into their response to load-induced deformations, failure mechanisms, and patterns of crack propagation. One of the crucial parameters for evaluating the structural behavior of reinforced concrete (RC) beams is the measurement of crack width and its progression. Numerous studies [22 - 24] have indicated that both crack width and propagation have the potential to diminish the stiffness of the beam, resulting in augmented deflections and decreased structural efficiency. The existence of wide cracks may lead to a reduction in the load-carrying capacity of the beam, thereby increasing the likelihood of premature structural failure. Besides, the occurrence of cracks can expose the embedded reinforcement to moisture, leading to the initiation of corrosion processes that jeopardize the structural integrity. In beams with low ductility, wide cracks can escalate the sus-

ceptibility to brittle failure. Additionally, the presence of cracks enables the penetration of water and aggressive substances, giving rise to durability concerns and possible deterioration of the structural elements [1].

This experimental study, sought to enhance the understanding of the strength and deformational characteristics of GFRP-reinforced beams under static loading conditions, thereby facilitating their effective application in structural engineering.

## 2. EXPERIMENTAL PROGRAM

### 2.1 Materials

The components that were integrated included fine aggregate, coarse aggregate, ordinary Portland cement, GFRP reinforcing bars, reinforcing steel bars as control and potable water. Fine aggregate comprised natural pit sand with a maximum particle size of 4.75mm, while coarse aggregate consisted of crushed granite with a maximum size of 12.5mm. Both fine and coarse aggregates underwent a sieve analysis that adhered to BS 1377: 1990 [25] standards, and the cement, met the specifications of ASTM C150 [26]. The GFRP bars were ribbed and sand coated, with diameters ranging from 10mm ~~to~~ 12mm (10 mm and 12mm). All the materials used in this experimental study including the GFRP bars were locally produced in Ghana, indicating the feasibility of implementing GFRP technology in the construction industry within the country.

### 2.2 Preparation of Test Specimens

#### 2.2.1 Mix design

Two concrete mix ratios were employed comprising 1:2:3, 0.45 and 1:1:2, 0.4 (cement: fine aggregate: coarse aggregate, w/c) for the intended concrete ~~grades~~ strength of C25 and C30 respectively in accordance with IS:10262 (1982) [27].

#### 2.2.2 Mixing, casting and curing

Initially, the fine aggregate and cement were proportioned and poured into a mechanical concrete mixer, followed by the addition of coarse aggregate. These materials were mixed in a dry state for around two minutes, after which water was gradually introduced to the dry

mixture. The mixing process was standardized, resulting in a consistent appearance in a plastic mix. To ensure thorough blending, the blending time was approximately 2 minutes per rotation. A slump test was performed to assess the workability of the concrete.

### 2.3 Preparation of GFRP Bars

The longitudinal tensile reinforcement ratios and transverse reinforcement ratio (stirrups) were parameters examined for the GFRP bars. Two longitudinal tensile reinforcement ratios of 0.7% (2ø12 mm GFRP bars) and 1.13% (3ø12 mm GFRP bars) together with a transverse shear reinforcement ratio of 0.85% (ø10mm, 200mm stirrup spacing) were adopted. The GFRP reinforcement ratios described above resulted in two configurations which are detailed in Fig. 1, in addition to the reinforcement cages fabricated. (What is the distance between the stirrups and the outer face of the beam? )

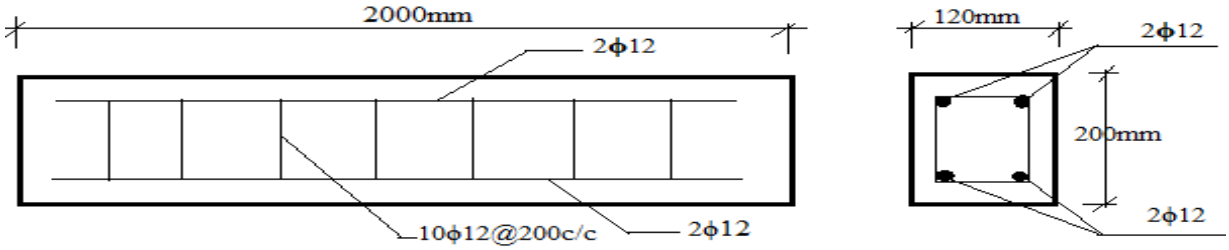


**(a) Beam configuration A**

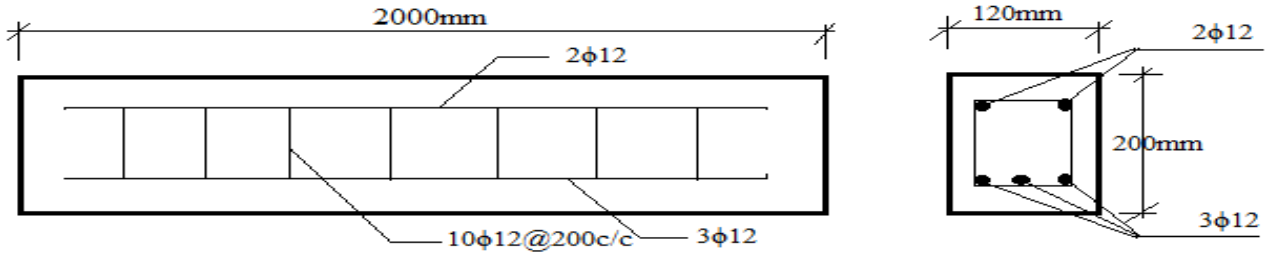


**(b) Beam configuration B**

**(c) Fabricated GFRP cages**

**Fig. 1. Preparation of reinforcement**

### 2.4 Preparation of Reinforced Concrete Beams

Marine board was employed as the material for the concrete beams and control specimen formwork, configured to specified dimensions of 120mm in width, 200mm in depth, and 2000mm in length for the beam. Lubrication was applied to the inner surface of the beam formwork using recycled engine oil to facilitate easy removal post-casting. After being filled with concrete and compacted, attention was given to achieving a consistent cover below and around the reinforcement, and the surface of the cast concrete was smoothened. A total of seven (7) beams were cast, with specific details provided in Table 1 (Present the data in sequence. Describe the table and then present it). Concrete cubes (150x150x150mm) and prisms (100x100x500mm) were cast as control for compressive strength and modulus of rupture respectively. After 24 hours, the beams and control specimens were extracted from their molds and subjected to a curing process under wet hessian cloth for 28 days. Prior to testing, they were thoroughly cleaned of any debris and coated with white emulsion paint on all surfaces.

### 2.5 Test Procedures

#### 2.5.1 Concrete compressive strength test

Compressive strength of the cured concrete cubes for both concrete mixes (1:2:3, 0.45 and 1:1:2, 0.4) was determined at 7 days, 14 days and 28 days in accordance with BS EN 12390-3 [29], using the Universal Testing Machine (UTM). The results of the concrete compressive

strength are shown in Table 2 (Present the data in sequence. Describe the table and then present it).

### 2.5.2 Concrete modulus of rupture test

The concrete prism (100mm x 100mm x 500mm) was simply supported over a span of 400mm in a study steel framework and loaded with a central point load until failure. The concrete modulus of rupture results ~~are~~ is presented in Table 3 (Present the data in sequence. Describe the table and then present it).

### 2.5.3 Tensile test

The tensile strength of the Glass Fiber Reinforced Polymer (GFRP) reinforcing bars was estimated by employing the Universal Testing Machine (UTM) based on the protocols specified in ASTM D7205 [30]. Specimens of 10mm and 12mm diameters were initially prepared by securing grip at each end with a 25mm steel pipe having an inner diameter of 22mm. The GFRP bars were inserted 150mm into the steel pipe grips at both ends, thus resulting in a 300mm free length. An epoxy mixture (Bisphenol A) enriched with expanding additives and distinguished by high-strength non-shrink properties was employed to fill the void between the steel pipe and GFRP bar. The specimens underwent a sealing process and were permitted to cure for a duration of 24 hours, followed by a subsequent three-day period for hardening.

The tensile test was carried out in a 1000 kN capacity ELE universal testing machine featuring an extensometer of 50mm gauge length. Tension was applied to the bar at a constant rate of 3mm per minute until failure. Various failure modes, including fiber glass fracture or epoxy failure were recorded, along with tensile strength, Young's modulus of elasticity, failure strain, and automatic plotting of stress-strain curve. Additionally, tensile test was conducted on the reinforcing steel bars. The results of tensile test are presented in Tables 4 and 5.

### 2.5.4 Testing of reinforced concrete beams

The cured beams at maturity of 28 days were cleaned and painted white in order to clarify the crack detection. The beams were placed in a rigid steel loading frame equipped with two supports positioned 100mm from the beam ends, with a clear span of 1,800mm (Indicate the distances between the loading actuators). An actuator comprising a hydraulic jack and an attached load cell was employed to apply the load at 2kN intervals. A shift spreader steel beam

was used to transfer the load to the specimen through two symmetrical loading points as illustrated in Fig. 2. The deflection and crack patterns were monitored, measured and recorded. At the failure loads, corresponding to the point of beam failure, the crack propagation parameters such as crack width, spacing and types of cracks were recorded for analysis. The recorded data were used to establish the load-deflection relationship and provide insights into beam behavior under the varying loads.

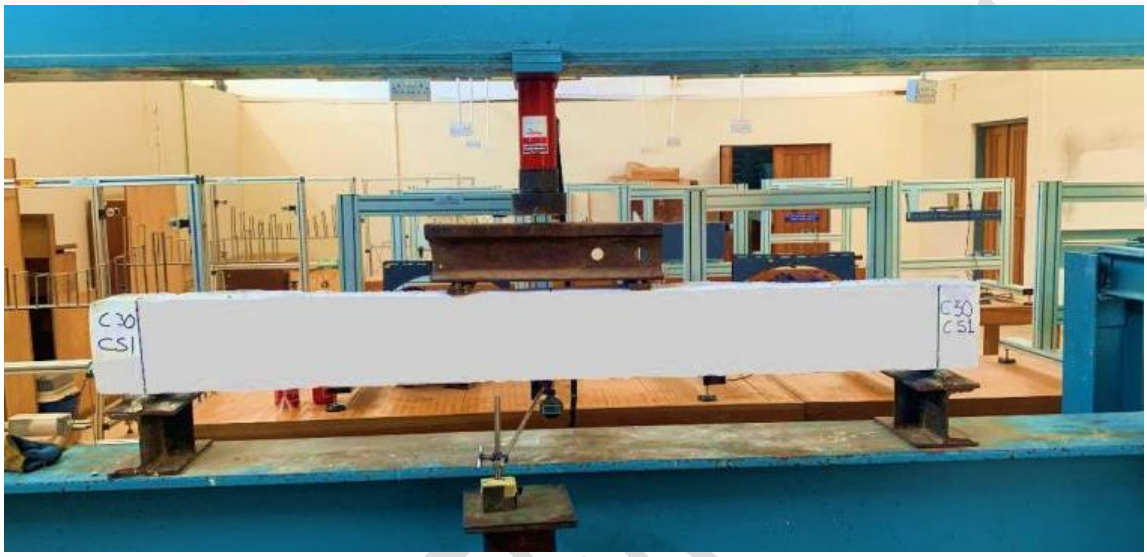


**Fig. 2. Beam Testing set-up**

**Table 1. Details of Beam specimens**

| S/N | Beam ID | Reinforcement Type | Cross-section b x d ($mm^2$) | Cube strength ($N/mm^2$) | Modulus of rupture ($N/mm^2$) | Compression reinforcement | | Tensile reinforcement | | Stirrups | |
|---|---|---|---|---|---|---|---|---|---|---|---|
| | | | | | | Ø (mm) | # | Ø(mm) | # | Ø(mm) | Spacing (mm) |
| 1 | C25/CS1 | GFRP | 120x200 | 23.4 | 5.4 | 12 | 2 | 12 | 2 | 10 | 200 |
| 2 | C30/CS1 | GFRP | 120x200 | 30.4 | 6.3 | 12 | 2 | 12 | 2 | 10 | 200 |
| 3 | C30/CS2 | GFRP | 120x200 | 30.4 | 6.3 | 12 | 2 | 12 | 2 | 10 | 200 |
| 4 | C25/ρ1 | GFRP | 120x200 | 23.4 | 5.4 | 12 | 2 | 12 | 3 | 10 | 200 |
| 5 | C25/ρ2 | GFRP | 120x200 | 23.4 | 5.4 | 12 | 2 | 12 | 3 | 10 | 200 |
| 6 | C25/ρ3 | GFRP | 120x200 | 23.4 | 5.4 | 12 | 2 | 12 | 3 | 10 | 200 |
| 7 | C25/S/200 | Steel | 120x200 | 23.4 | 5.4 | 12 | 2 | 12 | 3 | 10 | 200 |

(Indicate previously in the text what nomenclature refers to (CS, ρ and S)

**Table 2. Compressive strength of cube specimens**

| Specimen Target Strength | Average Compressive Strength (N/mm$^2$) | | |
|---|---|---|---|
| | 7 days | 14 days | 28 days |
| C25 | 16.3 | 20.9 | 23.4 |
| C30 | 20.1 | 27.1 | 30.4 |

**Table 3. Modulus of rupture of concrete prism specimens**

| Specimen Target strength | Average Maximum Load (N) | Average Modulus of Rupture (N/mm$^2$) |
|---|---|---|
| C25 | 9044.3 | 5.4 |
| C30 | 10463 | 6.3 |

## 3. RESULTS AND DISCUSSIONS

### 3.1 Mechanical properties of reinforcement bar specimens

The assessment was carried out to determine the mechanical characteristics of both conventional steel and Glass Fiber Reinforced Polymer (GFRP) bars utilized in reinforced concrete beams [7]. The 10mm bars were specifically employed as stirrups, whereas the 12mm bars served as the longitudinal reinforcement in the beam samples. The mechanical properties for the traditional mild steel bars and GFRP bars are presented in Tables 4 and 5 respectively. The 10mm and 12mm diameter GFRP bars exhibited ultimate tensile strengths of 1193 N/mm² and 1030 N/mm² respectively. The Young's modulus of elasticity of the GFRP bars were determined as 54.43 kN/mm² and 41.71 kN/mm² for the 10mm and 12mm bar sizes, respectively. Furthermore, the ultimate elongation values are recorded at 2.20% and 2.48% for the 10mm and 12mm GFRP bars, respectively. Furthermore, the stress-strain relationships of the GFRP bars are illustrated in Fig. 3.

**Table 4. Mechanical properties of traditional steel reinforcing bars**

| Bar ~~Size~~ Diameter | Average Diameter (mm) | Yield Strength ($N/mm^2$) | Yield Strain ($E_v$) | Tensile Strength ($N/mm^2$) | Average Ultimate Elongation (%) |
|---|---|---|---|---|---|
| 10mm | 9.24 | 464.20 | 0.0026 | 545.19 | 18.03 |
| 12mm | 11.17 | 457.57 | 0.0031 | 538.30 | 18.7 |

**Table 5. Mechanical properties of GFRP bars**

| Bar ~~Size~~ Diameter | Average Diameter (mm) | Average Ultimate Tensile Strength ($N/mm^2$) | Average Young's Modulus of Elasticity ($kN/mm^2$) | Average Ultimate Elongation (%) |
|---|---|---|---|---|
| 10mm | 9.54 | 1193 | 54.43 | 2.20 |
| 12mm | 11.35 | 1030 | 41.71 | 2.48 |

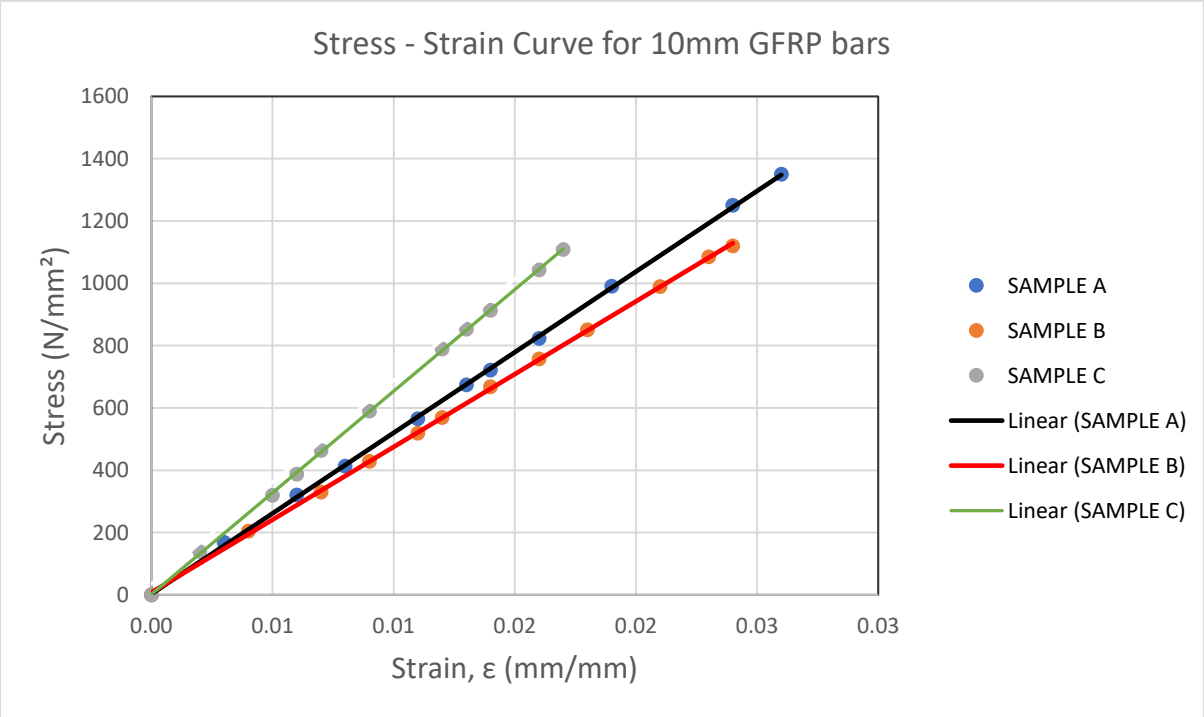

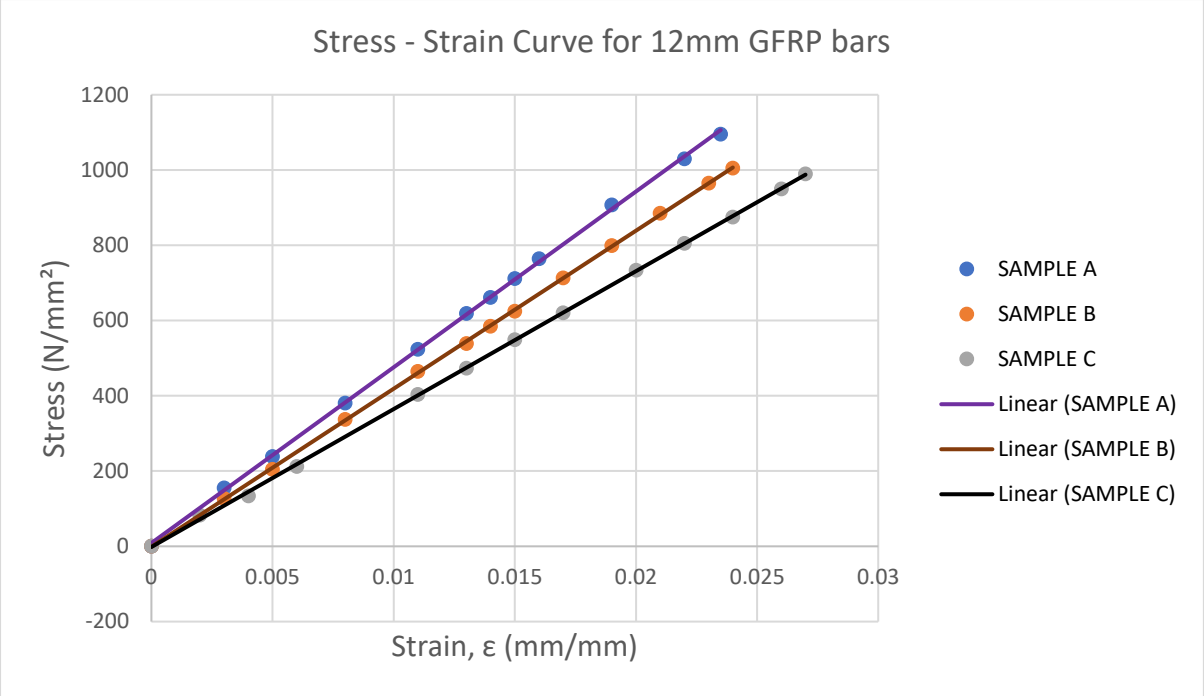


232

233 **Fig. 3. Stress-strain curve for 10mm and 12mm GFRP bars**

**Table 6. Deflections and crack modes**

| S/N | Beam ID | Deflection at first crack, (mm) | Final de-flection (mm) | Maximum crack width (mm) | Average crack spacing (mm) | Types and No. of cracks | | |
|---|---|---|---|---|---|---|---|---|
| | | | | | | No. of pure shear cracks | No. of flexural shear cracks | |
| | | | | | | | Within loaded span | At shear spans |
| 1 | C25/CS1 | 0.98 | 28.86 | 1 | 97.5 | 4 | 5 | 4 |
| 2 | C30/CS1 | 9.04 | 19.53 | 1 | 55.54 | 6 | 6 | 3 |
| 3 | C30/CS2 | 2.52 | 20.3 | 1 | 50.52 | 6 | 8 | 3 |
| 4 | C25/ρ1 | 5.19 | 19.88 | 0.5 | 71.88 | 5 | 6 | 3 |
| 5 | C25/ρ2 | 7.99 | 18.54 | 1 | 68.9 | 4 | 4 | 7 |
| 6 | C25/ρ3 | 4.66 | 20.38 | 0.5 | 91.57 | 3 | 6 | 5 |
| 7 | C25/S/200 | 4.43 | 11.39 | 2 | 54.83 | 6 | 7 | 9 |

## 3.4 THEORETICAL FLEXURAL ANALYSIS

(Briefly introduce what will be covered in the internal items in section 3.4)

### 3.4.1 Cracking moment

### 3.4.1 Cracking moment of reinforced concrete beam ($M_{cr}$)

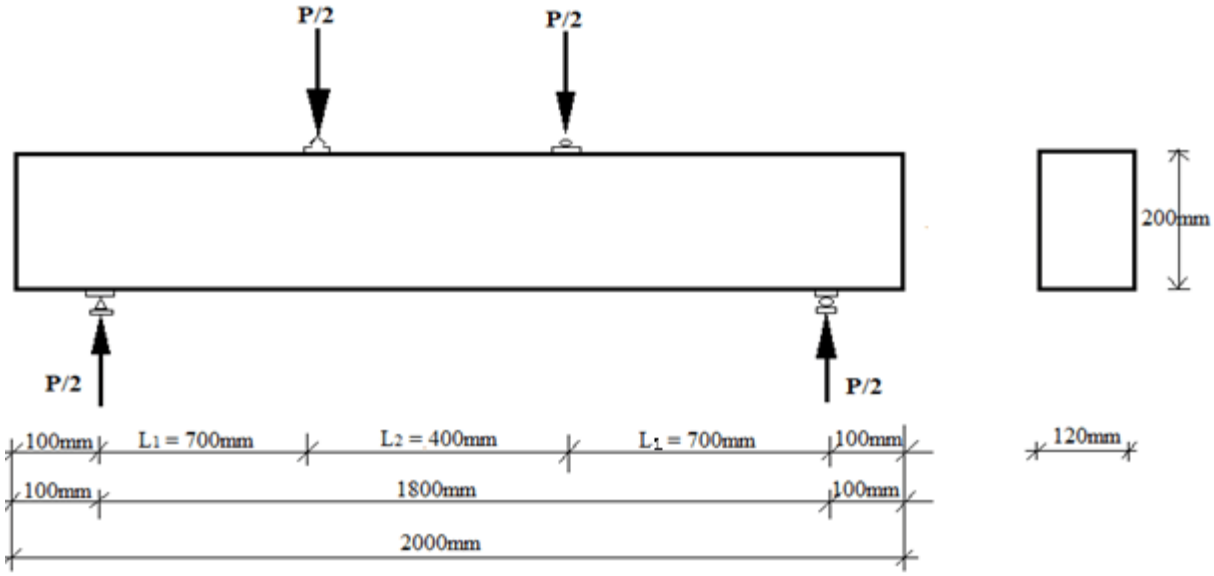


**Fig. 4. Schematic diagram of 4-point loading system for beams**

For a reinforced concrete beam, the cracking moment ($M_{cr}$) is obtained employing the modulus of rupture in the expression as in Eqn. 1, assuming elastic behaviour;

$$Cracking\ moment(M_{cr}) = f_t \mathrm{x} \frac{bd^2}{6} \ldots\ldots\ldots\ldots\ldots\ldots\ldots\ldots\ldots (1)$$

Suggestion

$$M_{cr} = f_t \frac{bd^2}{6} \ldots\ldots\ldots\ldots\ldots\ldots\ldots\ldots\ldots (1)$$

where $M_{cr}$ is the cracking moment (Nmm); $f_t$ is the modulus of rupture (N/mm$^2$); $b$ = width of beam (mm); $d$ = depth of beam (mm).

### 3.4.2 Theoretical cracking load of RC beam

From the 4-point loading system of the RC beam in Fig. 4., the theoretical cracking load of the beam can be expressed as shown in Eqn. 2;

$$P = \frac{2M}{L_1} \ldots\ldots\ldots\ldots\ldots\ldots\ldots\ldots\ldots\ldots (2)$$

where P = $P_{cr}$; $P_{cr}$ is the theoretical cracking load (kN); M = $M_{cr}$ is the cracking moment (kNm); $L_1$ is distance from the support to the nearest load point ~~(=700mm)~~ (700mm). Computed values of theoretical cracking loads for the RC beams are shown in Table 7.

### 3.4.3 Analyses of theoretical failure load

The analysis of the theoretical failure load is based on three main assumptions, namely; ( i ) GFRP bar failing first, ( ii ) concrete crushing first or ( iii ) shear failure occurring first.

### 3.4.4 Theoretical failure load based on GFRP bar failing first

For the simply supported shown in Fig. 4, the ultimate load is expressed by Eqn. 3 as follows;

$$P_{ult} = \frac{2M_{rf}}{L_1} \ldots\ldots\ldots\ldots\ldots\ldots\ldots\ldots\ldots (3)$$

where $M_{rf}$ is the moment of resistance of GFRP bar in tension (kNm); $P_{ult}$ is the ultimate failure load for GFRP bar (kN); $L_1$ is distance from the support to the nearest load point (=700mm).

With partial factor of safety of 1.52 [7], the moment of resistance of the GFRP in tension is given by;

$$M_{rf} = 0.66 f_{yf} A_f \text{ x } 0.775\text{d} \ldots\ldots\ldots\ldots\ldots\ldots\ldots (4)$$

where $f_y$ is the tensile strength of GFRP bar (N/mm$^2$); $A_f$ is area of GFRP in tension zone (mm$^2$); $d$ is the effective depth of beam (mm).

Three ~~(3)~~ categories of tensile reinforcement were employed in the beam specimen; namely; ratios of 0.7% and 1.13% GFRP bars and 0.7% steel tensile reinforcement in control beams are shown in Table 7.

### 3.4.5 Theoretical failure load based on concrete crushing first

Theoretical failure load of a reinforced concrete beam based on concrete crushing first in compression is given as expressed by Eqn. 6 including compression bar;

$$P_{ult} = \frac{2M_{rc}}{L} \ldots\ldots\ldots\ldots\ldots\ldots\ldots\ldots\ldots (5)$$

$$M_{rc} = 0.156 f_{cu} b d^2 + \gamma_m f_{fy} A_f (d - d^1) \ldots\ldots\ldots\ldots\ldots (6)$$

where $M_{rc}$ is the ~~M~~moment of resistance of concrete beam (kNm); $P_{ult}$ is the Concrete crushing load (kN); $f_{cu}$ is the concrete compressive strength (N/mm$^2$); $\gamma_m$ is the partial factor of safety; $d^1$ is the effective depth of compression GFRP bar; $A_f$ is the area of GFRP bars in compression. The computed values of failure loads of the RC beams assuming concrete crushes first are captured in Table 7 without contribution by GFRP bars in compression [17].

### 3.4.6 Theoretical failure load based on the assumption of shear failure occuring first

$$V_f = 0.66\frac{Asv}{Sv} f_y * d + V_c bd \ldots\ldots\ldots\ldots\ldots\ldots (6)$$

where $V_f$ the ~~S~~shear failure load; $f_y$ is the yield strength of GFRP stirrups; $V_c$ is the design concrete shear strength; $A_{sv}$ is the area of shear reinforcement; $S_v$ is the spacing of stirrups; $b$ is the width of the beam (Units?).

Results of the computations for shear failure occurring first for beam specimens are captured in Table 7.

301 **Table 7. Cracking and Failure loads of beams**

| S/N | Beam ID | Theoretical cracking load, $P_{cr}$ (kN) | Experimental cracking load, $P'_{cr}$ (kN) | Theoretical Failure load $P_{ult}$ (kN) based on | | | Experimental failure load, $P'_{ult}$ (kN) | $P'_{cr}/P_{cr}$ | $P'_{ult}/P_{ult}$ |
|---|---|---|---|---|---|---|---|---|---|
| | | | | GFRP failing | Concrete Crushing | Shear Failure | | | |
| 1 | C25/CS1 | 12.3 | 12 | 52.3 | 37.0* | 98.6 | 28 | 0.96 | 0.76 |
| 2 | C30/CS1 | 14.4 | 16 | 52.3 | 48.1* | 98.6 | 28 | 1.11 | 0.58 |
| 3 | C30/CS2 | 14.4 | 16 | 52.3 | 48.1* | 98.6 | 36 | 1.11 | 0.75 |
| 4 | C25/ρ1 | 12.3 | 14 | 78.6 | 37.0* | 98.6 | 30 | 1.14 | 0.81 |
| 5 | C25/ρ2 | 12.3 | 16 | 78.6 | 37.0* | 98.6 | 30 | 1.3 | 0.81 |
| 6 | C25/ρ3 | 12.3 | 16 | 78.6 | 37.0* | 98.6 | 28 | 1.3 | 0.76 |
| 7 | **C25/S/200 | 12.3 | 20 | 30.6* | 70.5 | 63.4 | 30 | 1.6 | 0.98 |
| ** Steel reinforced beam *Governing failure load of beam | | | | | | | Average: | 1.15 | 0.75 |

302 (This information should be in the table notes)

## 4. THEORETICAL AND EXPERIMENTAL RESULTS

### 4.1 Cracking moment

The cracking loads of the tested beams are detailed in Table 7. Specifically, the experimental cracking load values for the GFRP RC beams ranged from 12k N to 16 kN, whiles the steel reinforced beam had an experimental cracking load at 20 kN. The experimental cracking loads ($P'_{cr}$) of the beams reinforced with GFRP bars averaged 1.15 ~~(approximately 115 percent)~~ (15% higher ) of the theoretical cracking loads ($P_{cr}$). However, the beams reinforced with steel reinforcing bars achieved experimental cracking loads ($P'_{cr}$) 1.6 ~~(approximately 160 percent)~~ (60% higher) of the theoretical cracking loads ($P_{cr}$). It is noteworthy that the cracking load is closely associated with the tensile strength of concrete, a property dependent on compressive strength. As such, an increase in concrete compressive strength resulted in higher cracking moments.

### 4.2 Load-Deflection Behaviour

Fig. 5 illustrates typical bilinear load-deflection relationships for seven (7) reinforced concrete beams. Six (6) beams were reinforced with GFRP bars, while one (1) beam was reinforced with traditional mild steel bars. In general, the load-deflection curves of the GFRP RC beams can be categorized into two distinct phases; the initial phase is commonly known as the "pre-crack stage", during which the behavior exhibited by all beam specimens demonstrated a steep and nearly linear trend. Subsequently, the succeeding phase is referred to as the "post-cracking stage", characterized by the initiation and progression of cracks within the specimens. During this latter phase, the further crack propagation into the concrete compression zone led to a reduction in the flexural stiffness of the beams, until failure due mainly to concrete crushing.

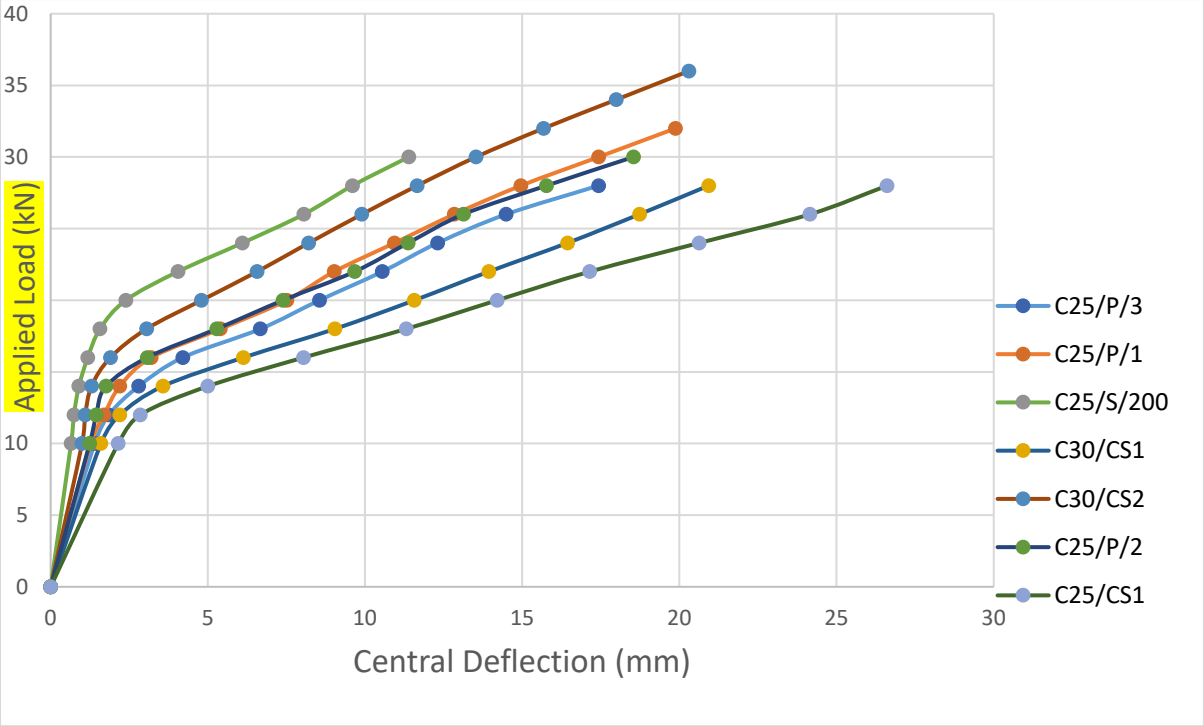


**Fig. 5. Load - deflection response (Adjust the graph)**

### 4.3 Crack Propagation and Crack Width

The investigation of crack width is a vital parameter in the assessment of the performance of reinforced concrete structures. At failure, Beam C25/CS1 developed 1mm maximum crack width, with average crack spacing of 97.5mm. This yielded a total of 13 number of cracks comprising 4 number of pure cracks, 5 number flexural cracks within the loaded span and 4 number flexural cracks within the shear span. Further details of the crack propagation are given in Table 6. As such, Table 6 illustrates that increasing reinforcing ratio in GFRP-RC beams led to an increase in the quantity of cracks and consequently a reduction in the average crack spacing. Additionally, Table 6 highlights the influence of concrete strength on the formation of cracks. Under identical load levels, higher concrete strength led to a greater number of cracks with reduced spacing and narrower crack widths compared to beams with lower concrete strength as confirmed by previous studies [11, 20].

(Rewrite and reorganize this sentence)

### 4.4 Failure Loads

Table 7 presents the theoretical and experimental failure loads of the beams under monotonic loading conditions. The average experimental failure load ($P'_{ult}$) of the GFRP RC beams were approximately 75% of the theoretical failure load ($P_{ult}$). On the other hand, the experimental

failure load ($P'_{ult}$) observed for the steel reinforced concrete beams was found to be 98% of the theoretical ultimate failure loads.

It can be observed from Table 7 that the experimental failure loads ($P'_{ult}$) of the GFRP RC beams ranged between 28 kN and 36 kN. Beam C30/CS2, with a compressive strength of 30.4 N/mm$^2$, exhibited a higher experimental failure load compared to beam C25/CS1, with compressive strength of 23.4 N/mm$^2$. This indicates that an increase in the concrete compressive strength of GFRP RC beams caused an increase in the failure load. Adam et al. [1] and Yang [5] also had similar findings. As depicted in Table 7, GFRP RC beam C25/CS1, with a longitudinal tensile reinforcement ratio of 0.7%, experienced a lower ultimate load of 28 kN in contrast to beam C25/ρ1, with a longitudinal tensile reinforcement ratio of 1.13%, which failed at 30 kN. This pattern demonstrates that a greater longitudinal reinforced GFRP RC beam results in a higher failure load, and vice versa.

### 4.5 Flexural Capacity and Mode of Failure

The simply supported beam in this study that is subjected to monotonic loading has a maximum constant bending moment and zero shear across the central span. The remaining two spans, on the other hand, experience maximum shear forces and varying bending moment magnitudes under different loads. The central span of each beam specimen was found to be the location of the first crack, indicating the location of the greatest strain. The GFRP-RC beams failed by concrete crushing. This was due to shear-bond failure, diagonal tension failure in the concrete, and flexural failure brought on by concrete crushing as reported by Xie et al. [20] and Kim [23]. On the other hand, the steel-RC beam failed due to yielding of the steel tension bars.

(Present the figures and then describe it)

**Fig. 6. Beam C25/CS1 failure mode**

For Beam C25/CS1 shown in Fig. 6, the beam had longitudinal tensile reinforcement ratio of 0.7%, a transverse reinforcement ratio of 0.65%, a 23.4 N/mm$^2$ cube strength and a 5.4 N/mm$^2$ modulus of rupture. The beam failed with 4 pure shear cracks, 5 flexural cracks within the constant moment span and 4 flexural cracks at the shear span area of the beam. A maximum crack width of 1mm was measured with an average crack spacing of 97.5mm. The first crack appeared at 12 kN loading with a corresponding deflection of 0.98mm. At 28 kN loading, the beam underwent a sudden brittle failure at a final deflection of 28.86mm.

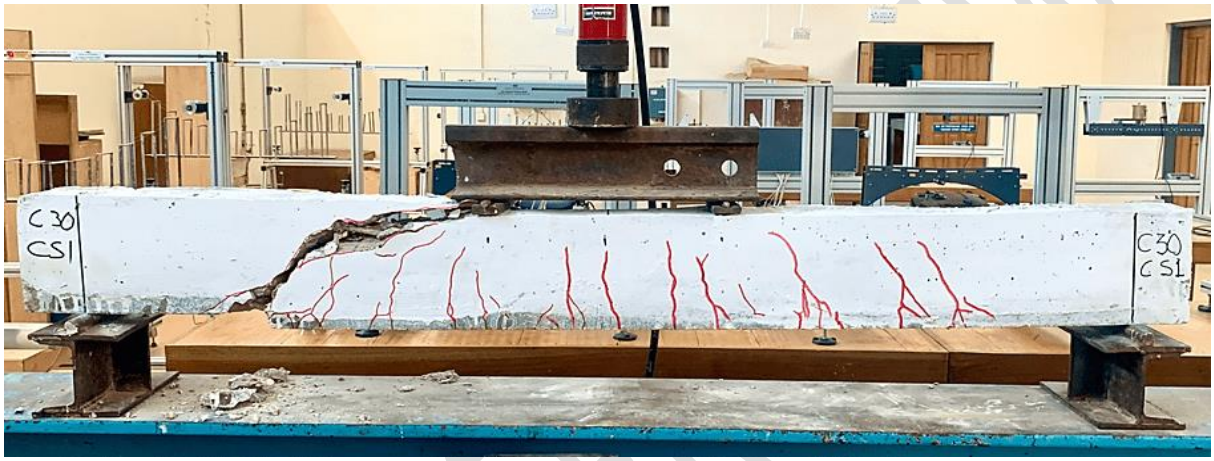


**Fig. 7. Beam C30/CS1 failure mode**

The Beam C30/CS1 in Fig. 7 had longitudinal tensile reinforcement ratio of 0.7%, a transverse reinforcement ratio of 0.65%, a 30.4 N/mm$^2$ cube strength and a 6.3 N/mm$^2$ modulus of rupture. The beam failed with 6 pure shear cracks, 6 flexural cracks within the loaded span and 3 flexural cracks at the shear span area of the beam. A maximum crack width of 1mm was measured with an average crack spacing of 55.45mm. The first crack appeared at 16 kN loading with a corresponding deflection of 9.04mm. At 28 kN loading, the beam underwent a sudden brittle failure at a final deflection of 19.53mm.

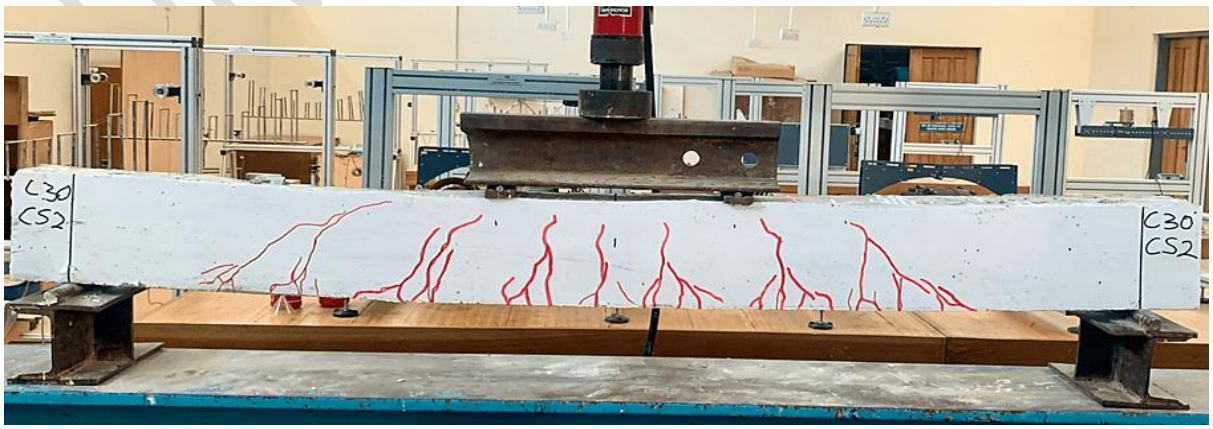

**Fig. 8. Beam C30/CS2 failure mode**

For Beam C30/CS2 in Fig.8, it had a longitudinal tensile reinforcement ratio of 0.7%, a transverse reinforcement ratio of 0.65%, a 30.4 N/mm$^2$ cube strength and a 6.3 N/mm$^2$ modulus of rupture. The beam failed with 6 pure shear cracks, 8 flexural cracks within the loaded span and 3 flexural cracks at the shear span area of the beam. A maximum crack width of 1mm was measured with an average crack spacing of 50.52mm. The first crack occurred at 16 kN loading with a corresponding deflection of 2.52mm. At 38 kN loading, the beam underwent a sudden brittle failure at a final deflection of 20.3mm.

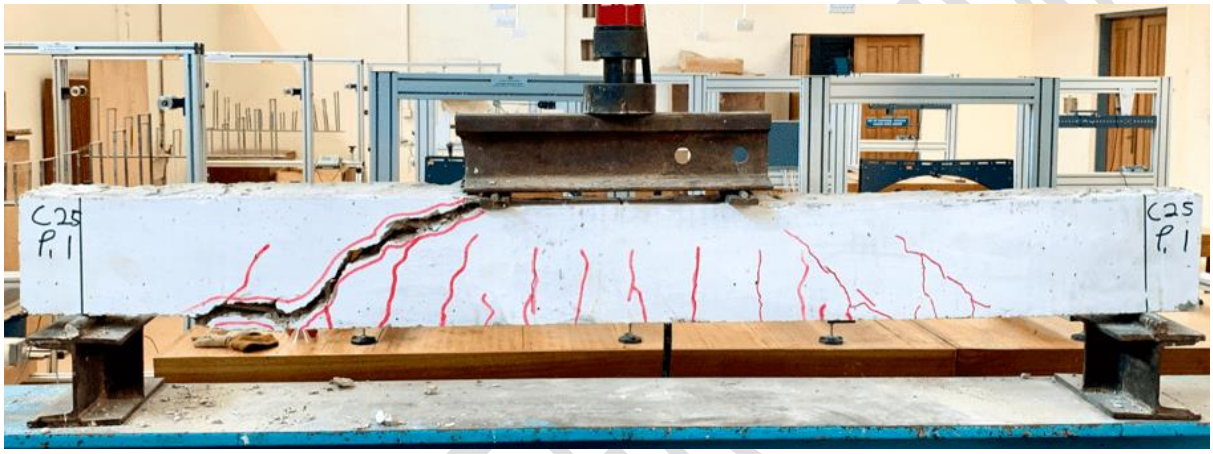


**Fig. 9. Beam C25/$\rho_1$ failure mode**

The Beam C25/$\rho_1$ in Fig.9 had a longitudinal reinforcement ratio of 1.13% (3 ~~No~~ø12mm GFRP bars in the tension zone), a transverse reinforcement ratio of 0.65% (stirrup spacing of 200mm), a 23.4 N/mm$^2$ cube strength and a 5.4 N/mm$^2$ modulus of rupture. The beam failed with 4 pure shear cracks, 4 flexural cracks within the loaded span and 7 flexural cracks at the shear span area of the beam. A maximum crack width of 1mm was measured with an average crack spacing of 71.88mm. The first crack appeared at 14 kN loading with a corresponding deflection of 7.99mm. At 30 kN loading, the beam experienced a sudden brittle failure at a final deflection of 15.54mm.

**Fig. 10. Beam C25/$\rho_2$ failure mode**

The Beam C25/$\rho_2$ in Fig. 10 had longitudinal tensile reinforcement ratio of 1.13% (3~~No~~ø12mm GFRP bars in the tension zone), a transverse reinforcement ratio of 0.65% (stirrup spacing of 200mm), a 23.4 N/mm$^2$ cube strength and a 5.4 N/mm$^2$ modulus of rupture. The beam failed with 5 pure shear cracks, 6 flexural cracks within the loaded span and 3 flexural cracks at the shear span area of the beam. A maximum crack width of 0.5mm was measured with an average crack spacing of 68.9mm. The first crack appeared at 16 kN loading with a corresponding deflection of 5.19mm. At 30 kN loading, the beam underwent a sudden brittle failure at a final deflection of 19.88mm.


**Fig. 11. Beam C25/$\rho_3$ failure mode**

The beam Beam C25/$\rho_3$ in Fig. 11 had longitudinal tensile reinforcement ratio of 1.13% (3~~No~~ø 12mm GFRP bars in the tension zone), a transverse reinforcement ratio of 0.65% (stirrup spacing of 200mm), a 23.4 N/mm$^2$ cube strength and a 5.4 N/mm$^2$ modulus of rupture. The beam failed with 3 pure shear cracks, 6 flexural cracks within the loaded span and 5 flexural cracks at the shear span area of the beam. A maximum crack width of 0.5mm was measured with an average crack spacing of 91.57mm. The first crack occurred at 16 kN loading with a corresponding deflection of 4.66mm. At 28 kN loading, the beam underwent a sudden brittle failure at a final deflection of 20.38mm.

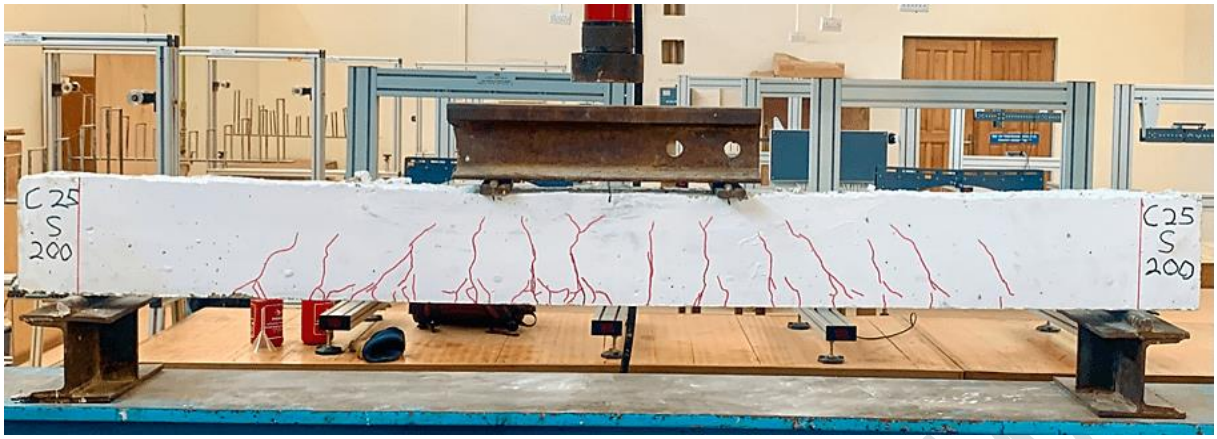


**Fig. 12. Beam C25/S/200 at failure**

Beam ID: C25/S/200 shown in Fig 12 is the control beam with traditional steel as reinforcement with same reinforcement configuration as the GFRP reinforced beams. The beam had longitudinal tensile reinforcement ratio of 0.7% (2-~~No~~ø 12mm steel bars in the tension zone), a transverse reinforcement ratio of 0.65% (stirrup spacing of 200mm), a 23.4 N/mm$^2$ cube strength and a 5.4 N/mm$^2$ modulus of rupture. The beam failed with 6 pure shear cracks, 7 flexural cracks within the loaded span and 9 flexural cracks at the shear span area of the beam. A maximum crack width of 2mm was measured with an average crack spacing of 54.83mm. The first crack occurred at 20 kN loading with a corresponding deflection of 4.43mm. At 30 kN loading, the beam underwent a sudden brittle failure at a final deflection of 11.39mm.

### 4.6 Effects of Concrete Strength on Structural Deformation of Beams Reinforced with GFRP Bars

Two strength grades of concrete were used in this experimental study, thus C25 and C30 which yielded compressive strength values of 23.4 N/mm$^2$ and 30.4N/mm$^2$ respectively. From Table 7, 23.4 N/mm$^2$ compressive strength of concrete achieved an estimated theoretical cracking load of 12.3 N/mm$^2$ compared to 14.4 N/mm$^2$ for 30.4N/mm$^2$, indicating a 17.1% increase in capacity of the GFRP RC beams. Similarly, beam ID C25/CS1 of 23.4 N/mm$^2$ compressive strength recorded 28 kN experimental load compared to beam ID C30/CS2 of 30.4 N/mm$^2$ compressive strength recorded higher values of 36 kN. A noticeable trend seen is that an increase in concrete strength from 23.4N/mm$^2$ to 30.4 N/mm$^2$ saw an increase in the load-carrying capacity by 28.6%. This finding is consistent with previous literature [4, 18] that found that higher concrete strength contributed to efficient utilization of GFRP bar and increased load-carrying capacity.

### 4.7 Effects of Longitudinal Tensile Reinforcement Ratio on Structural Deformation of Beams Reinforced with GFRP Bars

From Table 7, beam ID C25/CS1 with longitudinal tensile reinforcement ratio of 0.7% showed lower failure load compared to those with higher longitudinal tensile reinforcement ratio of 1.13% for GFRP bars. Similarly, GFRP reinforced beams with higher longitudinal ratio ($C25/\rho_1$, $C25/\rho_2$, $C25/\rho_3$ = 1.13%) recorded lower final deflections of 19.88mm, 18.54mm and 20.38mm respectively, compared to final deflections of 28.86mm, obtained from lower tensile reinforcement ratio of beam (C25/CS1, $\rho$=0.7%). This could be explained in light of the previous studies [9, 23], which confirmed the enhanced stiffness of the beams with increased tensile reinforcement ratio.

## CONCLUSIONS

This research investigated the structural behavior of concrete beams reinforced with GFRP bars as a promising alternative to conventional steel bars. The effects of variables of concrete compressive strength and tensile reinforcement ratios tested under a four-point monotonic loading system on the strength and deformational characteristics of GFRP-RC beams was examined. Based on the theoretical analysis and discussion of the experimental results, the following conclusions are drawn:

i. All GFRP reinforced concrete beams demonstrated typical bilinear elastic behavior until failure under static loading with evidence of reduced stiffness after cracking.

ii. The GFRP-reinforced concrete beams experienced sudden concrete crushing due to shear-bond failure, diagonal tension failure, and flexural failure, in contrast to the steel-reinforced concrete beam, which failed due to yielding of the steel tension bars, as confirmed by the theoretical analysis.

iii. For beam specimens reinforced with GFRP bars, an increase in concrete compressive strength from 23.4 kN to 30.4 kN resulted in a 28.6% increase in ultimate failure load.

iv. Under identical load levels, higher concrete strength led to a greater number of cracks with reduced spacing and narrower crack widths compared to beams with lower concrete strength.

v. For beams with similar compressive strength and tensile reinforcement ratios, GFRP-reinforced beams were seen to exhibit higher deflections and greater number cracks in comparison to beams reinforced with steel.

vi. Consistent with previous studies, increasing the longitudinal tensile reinforcement ratio ($\rho_w$) of GFRP from 0.7% to 1.13% greatly increased the ultimate flexural capacity of beam specimens. Additionally, reduced deflections were noted.

vii. Increasing the reinforcement ratio and concrete strength resulted in a larger number of cracks and smaller crack widths.

viii. When compared to conventional steel-reinforced beams, GFRP reinforced concrete beams showed improved flexural performance and hence a remarkable structural behavior under bending loads, despite their brittle behavior. (This can be reinforced with a ductility study of the beams)

**REFERENCES:**


[1] M. A. ; E. Adam Abeer M. ;. Habib, Fatma A. ;. El-Sayed, Taha A., "Structural Behavior of High-Strength Concrete Slabs Reinforced with GFRP Bars.," *Polymers*, vol. 13, no. 17, pp. 2997-NA, 2021, doi: 10.3390/polym13172997.

[2] S. A. ; K. Sheikh Zahra, "Replacement of steel with GFRP for sustainable reinforced concrete," *Construction and Building Materials*, vol. 160, no. NA, pp. 767–774, 2018, doi: 10.1016/j.conbuildmat.2017.12.141.

[3] G. B. ; M. Maranan Allan; Benmokrane, Brahim; Karunasena, Warna; Mendis, Priyan, "Evaluation of the flexural strength and serviceability of geopolymer concrete beams reinforced with glass-fibre-reinforced polymer (GFRP) bars," *Engineering Structures*, vol. 101, no. NA, pp. 529–541, 2015, doi: 10.1016/j.engstruct.2015.08.003.

[4] B. M. Tahmouresi Kasra; Mohseni, Ehsan, "Flexural response of FRP-strengthened lightweight RC beams: hybrid bond efficiency of L-shape ribbed bars and NSM technique," *Archives of Civil and Mechanical Engineering*, vol. 22, no. 2, p. NA-NA, 2022, doi: 10.1007/s43452-022-00410-y.

[5] J.-M. Y. Yang Doo Yeol; Shin, Hyun Oh; Yoon, Young Soo, “Flexural Strength and Deflection Evaluation for FRP Bar Reinforced HSC Beams with Different Types of Reinforcing Bar and Fiber,” *Journal of the Korea Concrete Institute*, vol. 23, no. 4, pp. 413–420, 2011, doi: 10.4334/jkci.2011.23.4.413.

[6] D. L. Shaoce Chenggao; Xian, Guijun, “Environmental Impacts of Glass- and Carbon-Fiber-Reinforced Polymer Bar-Reinforced Seawater and Sea Sand Concrete Beams Used in Marine Environments: An LCA Case Study,” *Polymers*, vol. 13, no. 1, pp. 154-NA, 2021, doi: 10.3390/polym13010154.

[7] G. O Boateng, C. K. Kankam, E. C. Mansal, R. O. Afrifa, F. Kwarteng, F. Ohene-Coffie, and S. A. K. Kpo. 2024. *“Evaluating the Mechanical Properties of Fiberglass-Reinforced Polymer Bar”.* Journal of Engineering Research and Reports 26 (7):150-60. https://doi.org/10.9734/jerr/2024/v26i71200.

[8] J. A. Lu Hamdy M. ;. Azimi, Hossein; Sennah, Khaled; Sayed-Ahmed, Mahmoud, “Bond characteristics of glass-fibre-reinforced polymer bars in high-strength concrete,” *Proceedings of the Institution of Civil Engineers - Structures and Buildings*, vol. 175, no. 10, pp. 748–764, 2022, doi: 10.1680/jstbu.19.00230.

[9] M. S. ; M. Issa Ibrahim M. ;. Elzeiny, Sherif M., “Influence of fibers on flexural behavior and ductility of concrete beams reinforced with GFRP rebars,” *Engineering Structures*, vol. 33, no. 5, pp. 1754–1763, 2011, doi: 10.1016/j.engstruct.2011.02.014.

[10] A. M. ; H. Erfan Hossam E. ;. Hatab, Khalil M. ;. El-Sayed, Taha A., “The flexural behavior of nano concrete and high strength concrete using GFRP,” *Construction and Building Materials*, vol. 247, no. NA, pp. 118664-NA, 2020, doi: 10.1016/j.conbuildmat.2020.118664.

[11] Sayan Sirimontree, Suraparb Keawsawasvong, and Chanachai Thongchom, “Flexural Behavior of Concrete Beam Reinforced with GFRP Bars Compared to Concrete Beam Reinforced with Conventional Steel Reinforcements,” **淡江理工學刊**, vol. 24, no. 6, Dec. 2021, doi: 10.6180/jase.202112_24(6).0009.

[12] R. P. Al-Sunna Kypros; Hajirasouliha, Iman; Guadagnini, Maurizio, “Deflection behaviour of FRP reinforced concrete beams and slabs: An experimental investigation,” *Composites Part B: Engineering*, vol. 43, no. 5, pp. 2125–2134, 2012, doi: 10.1016/j.compositesb.2012.03.007.

[13] H. D. Toutanji Yong, “Deflection and crack-width prediction of concrete beams reinforced with glass FRP rods,” *Construction and Building Materials*, vol. 17, no. 1, pp. 69–74, 2003, doi: 10.1016/s0950-0618(02)00094-6.

[14] Y. W. Chang Yanlei; Wang, Mifeng; Zhou, Zhi; Ou, Jinping, “Bond durability and degradation mechanism of GFRP bars in seawater sea-sand concrete under the coupling effect of seawater immersion and sustained load,” *Construction and Building Materials*, vol. 307, no. NA, pp. 124878-NA, 2021, doi: 10.1016/j.conbuildmat.2021.124878.

[15] Z. W. Dong Gang; Xu, Yi-Qian, “Experimental study on the bond durability between steel-FRP composite bars (SFCBs) and sea sand concrete in ocean environment,” *Construction and Building Materials*, vol. 115, no. NA, pp. 277–284, 2016, doi: 10.1016/j.conbuildmat.2016.04.052.

[16] J.-S. L. Jung Bang Yeon; Lee, Kang-Seok, “Experimental Study on the Structural Performance Degradation of Corrosion-Damaged Reinforced Concrete Beams,” *Advances in Civil Engineering*, vol. 2019, no. NA, pp. 1–14, 2019, doi: 10.1155/2019/9562574.

[17] S. A. Mohammed and A. I. Said, “A Comparative Study of the Structural Behavior of Concrete Beams Reinforced with Different Configurations of GFRP and Steel Bars,” *jcoeng*, vol. 30, no. 04, pp. 200–218, Apr. 2024, doi: 10.31026/j.eng.2024.04.12.

[18] M. A. Adam, M. Said, A. A. Mahmoud, and A. S. Shanour, “Analytical and experimental flexural behavior of concrete beams reinforced with glass fiber reinforced polymers bars,” *Construction and Building Materials*, vol. 84, pp. 354–366, Jun. 2015, doi: 10.1016/j.conbuildmat.2015.03.057.

[19] L. Z. Zhang Yu; Shaowei, Hu; Yang, Jiasheng; Xia, Lipeng, “Identification of Bond-Slip Behavior of GFRP-ECC Using Smart Aggregate Transducers,” *Frontiers in Materials*, vol. 7, no. NA, pp. 165-NA, 2020, doi: 10.3389/fmats.2020.00165.

[20] F. Xie, W. Tian, P. Diez, S. Zlotnik, and A. G. Gonzalez, “Bonding Performance of Glass Fiber-Reinforced Polymer Bars under the Influence of Deformation Characteristics,” *Polymers*, vol. 15, no. 12, p. 2604, Jun. 2023, doi: 10.3390/polym15122604.

[21] M. A. Muhammad Faris R. ;. Rafiq, Serwan, “Investigation of Flexural Performance of Concrete Beams Reinforced with Glass Fiber Reinforced Polymer Rebars,” *The Journal of the University of Duhok*, vol. 23, no. 2, pp. 630–647, 2020, doi: 10.26682/csjuod.2020.23.2.49.

[22] K. G. Pilakoutas Maurizio; Neocleous, Kyriacos; Matthys, Stijn, “Design guidelines for FRP reinforced concrete structures,” *Proceedings of the Institution of Civil Engineers*

- *Structures and Buildings*, vol. 164, no. 4, pp. 255–263, 2011, doi: 10.1680/stbu.2011.164.4.255.

[23] S.-E. K. Kim Seung-Hun, "Flexural behavior of concrete beams with steel bar and FRP reinforcement," *Journal of Asian Architecture and Building Engineering*, vol. 18, no. 2, pp. 89–97, 2019, doi: 10.1080/13467581.2019.1596814.

[24] H. Q. J. Ahmed Dilshad Kakasor; Yaseen, Sinan Abdulkhaleq, "Flexural Capacity and Behaviour of Geopolymer Concrete Beams Reinforced with Glass Fibre-Reinforced Polymer Bars," *International Journal of Concrete Structures and Materials*, vol. 14, no. 1, pp. 1–16, 2020, doi: 10.1186/s40069-019-0389-1.

[25] British Standards Institution. BSI. 1377 Part 1 (1990): General Requirement and Sample Preparation. British Standard Institute, London; 1990.

[26] ASTM. ASTM C150: Standard Specification for Portland Cement. Annual Book of ASTM Standards; 2001.

[27] Indian standard, Recommended Guidelines for Concrete Mix Design, IS 10262:1982, Bureau of India Standard, New Delhi.

[28] ACI 440.1R-15, Guide for the Design and Construction of Structural Concrete Reinforced with Fiber-Reinforced Polymer Bars, ACI Committee 440, 2015.

[29] BS EN 12390-3 (2009). Testing hardened concrete-Part 3: Compressive Strength of Test Specimens. British Standard Institution, London; 2009.

[30] ASTM D7205 (2006). Standard Test Method for Tensile Properties of Fiber Reinforced Polymer Matrix Composite Bars. ASTM Committee D30; 2006.